AgriEngineering

MDPI

Article

Mechanized Ground Roughness Mapping by Remotely Piloted Aircraft

Lucas Gabryel Maciel dos Santos [1], Lucas Santos Santana [1], Marcos David dos Santos Lopes [1], Josiane Maria da Silva [1], Carmem Lúcia da Silva Surmani [1], Celine Russo [2], Daniele Sarri [2], Giuseppe Rossi [2] and Andrea Pagliai [2,*]

[1] Institute of Agricultural Sciences (ICA), Federal University from Jequitinhonha and Mucuri's Valleys (UFVJM), Av. Universitária, n°1000, Unaí 38610-000, MG, Brazil; lucas.gabryel@ufvjm.edu.br (L.G.M.d.S.); santana.santos@ufvjm.edu.br (L.S.S.); marcos.david@ufvjm.edu.br (M.D.d.S.L.); silva.josiane@ufvjm.edu.br (J.M.d.S.); carmem.surmani@ufvjm.edu.br (C.L.d.S.S.)

[2] DAGRI—Department of Agriculture Environment Food and Forestry, Biosystem Engineering Division, University of Florence, Piazzale delle Cascine 15, 50144 Firenze, Italy; celine.russo@unifi.it (C.R.); daniele.sarri@unifi.it (D.S.); giuseppe.rossi@unifi.it (G.R.)

* Correspondence: andrea.pagliai@unifi.it

Abstract

Digital Elevation Models (DEMs) provide essential information for decision-making in precision agriculture. This study evaluated the altimetric quality of DEMs generated by Remotely Piloted Aircraft (RPA) platforms, the influence of flight direction, and the effect of mechanically disturbed soil surface conditions. We obtained data from a 900 m² area. Flights were conducted under pre- and post-mechanization conditions using a reversible plow, with flights in both longitudinal and transverse directions. We processed images using Structure-from-Motion (SfM) techniques to generate dense point clouds and DEMs. Statistical analyses relied on raster statistics and elevation cross-section transects of microtopography, were evaluated via descriptive statistics, ANOVA, Tukey's HSD tests, and spatialization with micro-variation classification. Significant differences emerged among the evaluated models ($p < 0.001$), with Phantom-derived DEMs showing systematically higher elevations than Mavic models (617.31 ± 0.16 m vs. 605.41 ± 0.23 m, respectively). Post-plowing longitudinal flights showed the least variation, indicating greater altimetric consistency after secondary soil preparation. Conversely, the pre-plowing transverse flight (Mavic Flight 2) produced the largest errors. Quantitative assessment of topographic profiles revealed high morphological correspondence between platforms, with Pearson correlation coefficients ranging from 0.84 to 0.96 after vertical normalization, confirming that terrain morphology was preserved despite systematic vertical offsets. The effect of flight direction was more pronounced before soil preparation; after harrowing (a homogeneous surface), the difference between directions decreased, but longitudinal flights maintained an advantage, while transverse flights (especially Mavic) tended to overestimate elevations spatially.

Keywords: photogrammetry; remote sensing; altimetric accuracy; digital agriculture; soil surface

Academic Editors: Muhammad Sultan, Yuguang Zhou, Redmond R. Shamshiri and Muhammad Imran

Received: 27 May 2026
Revised: 19 June 2026
Accepted: 21 June 2026
Published: 23 June 2026

1. Introduction

Agriculture is continually challenged to increase productivity sustainably, requiring technologies that improve decision-making and resource-use efficiency [1,2]. In this context, the incorporation of digital technologies has driven the modernization of agricultural practices, particularly precision agriculture, which uses geospatial data for site-specific crop management [3,4]. This approach enables the characterization of spatial and temporal variability in soil, topographic, and environmental conditions, supporting targeted interventions and the more efficient use of agricultural inputs [5]. Within this framework, detailed terrain mapping is essential, as microtopography directly influences processes such as drainage, erosion, and soil moisture distribution. Consequently, geospatial techniques have become essential tools for improving analytical and operational precision in agriculture [6,7]. The integrated use of remote sensing, Geographic Information Systems (GIS), and spatial analysis has expanded the applications of environmental and agricultural monitoring across different spatial scales [8].

Recent advances in geospatial technologies and the increasing availability of high-resolution data have expanded the acquisition, processing, and analysis of spatial information across multiple domains [9,10]. In this context, airborne remote sensing has been extensively explored due to its remarkable technological evolution over recent decades [11]. In precision agriculture, Remotely Piloted Aircraft (RPAs) stand out for enabling high-resolution imagery acquisition, operational flexibility, and relatively low operational costs [12,13]. These platforms enable the generation of fundamental cartographic products, such as Digital Elevation Models (DEMs), which numerically represent the terrain surface and are essential for analyzing agricultural operations, hydrological and erosive processes, and soil moisture dynamics [14]. The integration of remote sensors, digital modeling, and intelligent systems has further expanded the potential of digital tools to support agricultural decision-making [15].

DEM generation is primarily performed using active non-photogrammetric sensors, particularly LiDAR (Light Detection and Ranging), which is widely employed for highly detailed three-dimensional reconstruction [16,17]. Owing to the high complexity of the data and the elevated cost associated with this system, its applications in agriculture remain limited, highlighting the relevance of lower complexity DEMs that can still meet agricultural demands, such as point clouds from RGB sensors [18]. RGB cameras are recognized for their low cost and simplified data processing. Therefore, data from this type of sensor may be promising for applications across different farming scales, from family farming systems to large commercial farms. However, for effective integration into agricultural management, a comprehensive assessment is required, since the quality of DEMs obtained from RPAs is influenced by several factors, including the type of aerial platform, onboard sensors, flight parameters (altitude, speed, and image overlap), and the adopted photogrammetric processing methods [19,20]. Advances in digital technologies applied to agriculture have supported more sustainable and efficient approaches for monitoring and managing agricultural areas [21].

The interaction among these variables may result in products with different levels of vertical accuracy, directly affecting their reliability for precision agriculture applications [22]. In this context, the systematic evaluation of these models' performance is essential to ensure their suitability for technical and scientific applications. Furthermore, comparative studies are crucial for understanding the limitations and potentialities of DEMs generated from RPAs [23], since the lack of standardization in acquisition and processing procedures may result in significant variations in precision within the same study area [24].

Surface DEM generation may help address an important gap in agricultural mechanization, namely, the mapping of soil surface roughness after tillage operations.

https://doi.org/10.3390/agriengineering8070256

The use of highly detailed surface characterization remains poorly explored, whereas applications involving RPAs have been systematically focused on the classification of plant attributes. Nevertheless, understanding surface behavior following mechanized operations using low-cost sensors is essential for developing protocols to assess mechanization quality, particularly in soil disturbance operations such as plowing and harrowing.

Although RPA-based DEMs have been widely applied in precision agriculture, the influence of platform characteristics, flight direction, and soil surface conditions on DEM elevation consistency and roughness representation remains insufficiently understood [25]. In particular, it is still unclear whether different RPA platforms reproduce the same microtopographic patterns under mechanically disturbed conditions and how flight orientation relative to tillage-induced surface structures affects DEM consistency. Therefore, the central scientific question addressed in this study is how different RPA platforms, flight directions, and soil surface conditions resulting from mechanized tillage influence DEM elevation consistency and the representation of agricultural surface roughness. Understanding these factors is essential for establishing standardized acquisition protocols and improving the reliability of RPA-derived DEMs for agricultural mechanization assessment and precision agriculture applications [17,26].

Given this scenario, the present study evaluates the relative elevation consistency and morphological representation of Digital Elevation Models generated from RPAs widely used in agriculture, considering platform characteristics, flight directions, and soil surface conditions before and after mechanized tillage. The analysis focuses on comparing DEM behavior under different acquisition conditions, emphasizing systematic vertical offsets and terrain morphology preservation rather than absolute vertical accuracy, since no external ground-reference measurements were available.

2. Materials and Methods

2.1. Data Acquisition

The experiment was conducted at the Santa Paula Experimental Farm (FESP) of the Federal University of the Jequitinhonha and Mucuri Valleys, Unaí Campus, Minas Gerais, Brazil, in an area classified as a Red Latosol, covering approximately 900 m^2 (Figure 1).

The evaluated experimental area presented a surface recently disturbed by mechanized soil tillage operations, a condition considered fundamental for the analysis of surface roughness using RPAs. The mechanized operation was performed using a New Holland TT4.75 agricultural tractor coupled to a four-disk hydraulic reversible plow with 28-inch disks, a working width of 1.10 m, an operational depth of approximately 0.35 m, and a mass of approximately 760 kg. The implement operation promoted intense mobilization of the soil surface layer, resulting in microtopographic variations, furrows, and aggregates that favored the generation of roughness patterns compatible with high-resolution altimetric analyses. This experimental condition enabled the evaluation of the potential of RPAs to detect and map surface roughness induced by mechanized operations, aligning the study with the monitoring of soil physical attributes.

Aerial images were acquired using two Remotely Piloted Aircraft (RPAs): the DJI Mavic 3 Multispectral (DJI, Shenzhen, China) (Figure 1C) and the DJI Phantom 4 Multispectral (DJI, Shenzhen, China) (Figure 1D), selected for their complementary sensors, spatial resolution, and flight capabilities (Table 1). The DJI Mavic 3 Multispectral integrates an RGB camera with a four-band multispectral sensor, enabling high-precision small-scale mapping. The Phantom 4 Multispectral is equipped with a higher-resolution RGB camera and a five-band multispectral sensor, making it better suited for detailed surveys and data acquisition under different flight conditions.

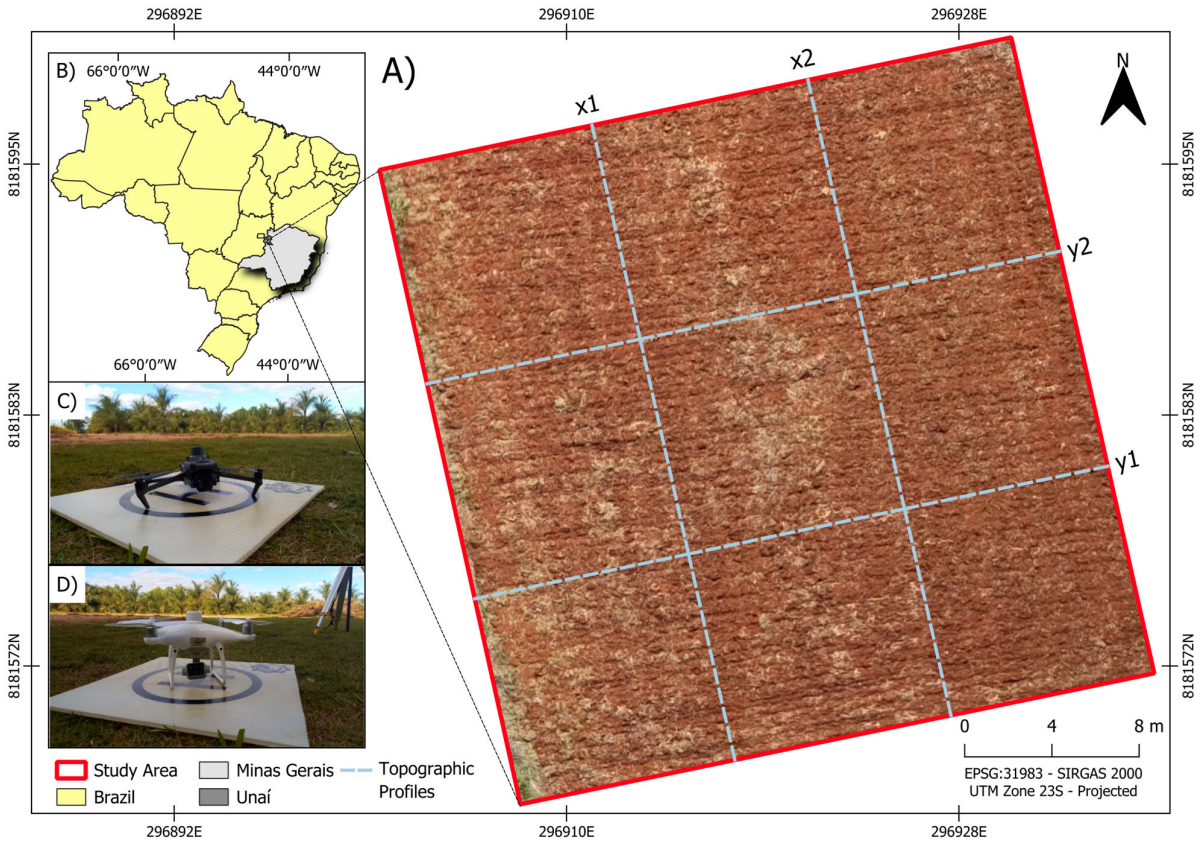

Figure 1. Experimental area and transects used for topographic profile extraction. (**A**) Study area and profile sampling lines along the X- and Y-axes; (**B**) location of the experimental area in Unaí, Minas Gerais, Brazil; (**C**) DJI Mavic 3 Multispectral; and (**D**) DJI Phantom 4 Multispectral.

Table 1. Comparison of technical specifications of the DJI Mavic 3 Multispectral and DJI Phantom 4 Multispectral.

Characteristic	DJI Mavic 3 Multispectral	DJI Phantom 4 Multispectral
RGB sensor	20 MP	48 MP
Multispectral sensor	4 CMOS 1/2.8″ sensors (5 MP)	5 CMOS 1/2.9″ sensors (2.12 MP)
Lens	25 mm, f/2.0, FOV 73.91°	5.74 mm, f/2.2, FOV 62.7°
Shutter	1/2000 s	Up to 1/8000 s
Spectral bands	Green (560 ± 16 nm), Red (650 ± 16 nm), RedEdge (730 ± 16 nm), NIR (860 ± 26 nm)	Blue (450 ± 16 nm), Green (560 ± 16 nm), Red (650 ± 16 nm), RedEdge (730 ± 16 nm), NIR (840 ± 26 nm)

Flight planning was conducted to maximize spatial resolution and the quality of the Digital Elevation Models (DEMs), using the minimum operational altitudes permitted by the aircraft's collision-avoidance sensors. For the DJI Phantom 4 Multispectral, flights were performed at 15 m above ground level (AGL), with a speed of 1.0 m s^{-1}, resulting in a Ground Sample Distance (GSD) of 0.80 cm $pixel^{-1}$, 80% frontal overlap, and 70% lateral overlap. For the DJI Mavic 3 Multispectral, flights were conducted at 12 m AGL while maintaining the same speed and overlap percentages, resulting in a GSD of 0.55 cm $pixel^{-1}$.

Six flights were conducted for each RPA between 10:00 a.m. and 1:00 p.m., with an approximate 35 min interval between missions. Flights were identified by the aircraft name followed by sequential numbering corresponding to the chronological order of execution (e.g., "Mavic 1"). Throughout all operations, the camera remained oriented to

nadir (−90°), ensuring vertical image acquisition, complete coverage of the study area, and high data redundancy.

A DJI D-RTK 2 base station was used to establish high-precision coordinate correction during all surveys. The base station was initialized approximately 20 min before each flight to ensure signal stabilization and centimeter-level positioning accuracy. No ground control points (GCPs) were installed in the experimental area, and georeferencing was based exclusively on the onboard GNSS/RTK systems of each RPA operating under real-time correction. Image coordinates were directly used in Agisoft Metashape (version 2.3.1), and the DEMs were therefore generated under direct georeferencing conditions and evaluated in terms of relative elevation consistency among platforms and flight configurations. All data were processed in the UTM coordinate system referenced to the SIRGAS 2000 datum, with elevations expressed as ellipsoidal heights.

2.2. Processing

The acquired images were processed in Agisoft Metashape using a standardized photogrammetric workflow configured to achieve maximum quality at all processing stages. Image alignment was performed with the "Highest" accuracy, using a limit of 80,000 key points and 8000 tie points, aiming to maximize feature correspondence and the geometric precision of the photogrammetric block. Dense point cloud generation was conducted using "Ultra High" quality, with depth filtering set to "Mild," preserving the highest possible level of surface detail. Subsequently, the Digital Elevation Models (DEMs) and orthomosaics were generated at maximum resolution using interpolation enabled, the "Mosaic" blending mode, and automatic color correction.

Camera calibration was automatically performed in Agisoft Metashape during image alignment. Alignment quality was assessed through reprojection errors and tie-point distribution, and DEMs were exported in GeoTIFF format without additional vertical transformations or datum conversions.

For the quantitative analysis of the Digital Elevation Models (DEMs), a script was developed in the R environment using the raster, ggplot2, and reshape2 packages. The script was responsible for automated raster file reading, systematic sampling of 1000 random georeferenced points, and extraction of corresponding elevation values from all 12 DEMs. Following rigorous quality control, points containing missing values (NA) in any model were removed, resulting in 999 valid points for comparative analyses. The data were converted to long format and subjected to descriptive statistical analysis, including mean, median, standard deviation, minimum, and maximum values. Subsequently, a one-way analysis of variance (ANOVA) was performed, followed by Tukey's HSD multiple-comparison test ($p < 0.05$), to identify statistically significant differences among the models.

For the spatialized altimetric mapping analysis, all DEM rasters were standardized in a GIS environment to ensure comparability among models generated by different platforms and flight conditions. A reference value of 600 m, lower than the minimum elevation observed in all DEMs, was adopted as a common baseline for normalization. This procedure was used exclusively to remove absolute elevation offsets and facilitate comparisons of relative spatial patterns among models, without representing a physical elevation benchmark. Subsequently, the normalized rasters were reclassified into three equidistant altimetric intervals using table-based reclassification. The resulting classes were vectorized into polygon format for quantifying the occupied area (m^2) within each interval, enabling a standardized comparison of surface spatial organization across flights and platforms.

Additionally, a second script was developed to extract and analyze topographic profiles from the DEMs, enabling the evaluation of the spatial behavior of surface roughness and altimetric variations across the experimental area. The procedure consisted of loading the DEMs, converting the rasters into georeferenced data frames, and automatically defining equidistant profiles along the X- and Y-axes. Profiles were extracted from sampling strips with widths corresponding to 2% of the total area extent, using aggregated elevation averages to reduce local noise.

Subsequently, high-resolution faceted plots were generated, and the profiles were exported as .csv files and image outputs, enabling detailed analysis of surface continuity and the topographic response of the generated models. To separate systematic vertical offsets from terrain morphology, relative elevation profiles were also generated by subtracting the mean elevation of each profile from all profile observations. This normalization allowed the comparison of profile shapes independently of absolute elevation differences.

3. Results

3.1. Altimetric Comparison Among Digital Elevation Models

The analysis of variance (ANOVA) revealed highly significant differences among the evaluated Digital Elevation Models (DEMs) ($p < 0.001$), indicating a strong effect of the model on the obtained elevation values (Table 2). The high F-value (535,453), associated with the low residual mean square (MS = 0.042), demonstrates low internal variability among samples and high separation among the analyzed groups, evidencing statistical consistency among the models generated under different platforms and flight conditions.

Table 2. Analysis of variance (ANOVA) for model comparison.

Source of Variation	df	SS	MS	F	*p*-Value
Model	7	157,271	22,467.297	535,453	<0.001
Residuals	7984	335	0.0420	–	–

df: degrees of freedom; SS: sum of squares; and MS: mean square.

Descriptive statistics revealed systematic differences between the models derived from the Mavic and Phantom platforms (Table 3). Phantom models showed higher mean elevations across all evaluated campaigns. The highest mean value was observed for Flight 2 Phantom (617.31 ± 0.16 m), followed by Flight 1 Phantom (617.21 ± 0.16 m), whereas the lowest value was recorded for Flight 2 Mavic (605.41 ± 0.23 m). The total range between the elevation extremes reached approximately 11.9 m, evidencing substantial vertical discrepancies between the platforms. Despite these absolute differences, all models presented low internal dispersion, with standard deviations ranging from 0.15 to 0.27 m. The low standard deviations indicate high internal stability of the evaluated models.

Table 3. Descriptive statistics of the evaluated models.

Model	Direction	Mean (m) ± SD	Min. (m)	Max. (m)
Flight 1 Mavic	Longitudinal	607.49 ± 0.27	606.90	608.13
Flight 1 Phantom	Longitudinal	617.21 ± 0.16	616.81	617.53
Flight 2 Mavic	Transversal	605.41 ± 0.23	604.89	606.02
Flight 2 Phantom	Transversal	617.31 ± 0.16	616.94	617.62
Flight 3 Mavic	Longitudinal	608.82 ± 0.23	608.32	609.42
Flight 3 Phantom	Longitudinal	614.87 ± 0.15	614.46	615.15
Flight 4 Mavic	Transversal	608.66 ± 0.24	608.11	609.21
Flight 4 Phantom	Transversal	614.98 ± 0.16	614.58	615.26

Pairwise comparisons between Phantom and Mavic models using Tukey's HSD test confirmed significant differences across all evaluated flights (Table 4). Flight 2 presented the greatest mean discrepancy between platforms, with a difference of 11.908 ± 0.0065 m ($p < 0.001$), followed by Flight 1, with a mean difference of 9.721 ± 0.0065 m. Flights 3 and 4 showed smaller, yet still significant, differences of 6.047 ± 0.0065 m and 6.326 ± 0.0065 m, respectively.

Table 4. Pairwise mean elevation differences (m) between Phantom and Mavic drones across four flights, based on Tukey's HSD post hoc test.

Contrast (Phantom—Mavic)	Mean Difference ± SE (m)	95% CI (m)	*p*-Value
Flight 1	9.721 ± 0.0065	9.693–9.749	<0.001
Flight 2	11.908 ± 0.0065	11.880–11.936	<0.001
Flight 3	6.047 ± 0.0065	6.019–6.074	<0.001
Flight 4	6.326 ± 0.0065	6.298–6.353	<0.001

SE = √(MS_residual/n), with MS_residual = 0.042 and n = 999. CI: 95% confidence interval. Critical value: q(0.05; 8; 7984) = 4.286. *p*-values were adjusted for 28 comparisons. Positive values indicate higher elevations in Phantom DTMs.

The 95% confidence intervals had low amplitude across all contrasts, indicating high precision of the estimates. All contrasts showed positive values, indicating that Phantom models systematically produced higher surfaces than Mavic models. The observed differences between Phantom and Mavic DEMs indicate a systematic vertical offset (z-shift) of approximately 6–12 m. However, the preservation of profile morphology suggests that both platforms consistently represented the same terrain features.

The reduction in vertical discrepancies after harrowing indicates greater consistency among the generated models, possibly due to the formation of a more homogeneous surface roughness pattern following soil disturbance. This condition reduced local surface variability, leading to improved relative elevation consistency across the DEMs. The results also showed that flight direction influenced DEM consistency and the magnitude of vertical offsets, particularly during the pre-harrowing period, when transversal flights exhibited greater vertical discrepancies than longitudinal flights.

3.2. Extraction of Topographic Profiles from the Digital Elevation Models

The analysis of elevation profiles generated by the Mavic and Phantom systems (Figure 2) demonstrated substantial vertical variations among the different flight missions, both within the same platform and between the two systems. Along the X-axis (Position 1), the data collected by the Mavic sensor showed considerable oscillation. While Flight 1 initiated the profile at 607.59 m, Flight 2 recorded 605.45 m at the same coordinates. In subsequent missions, the values increased again, reaching 608.90 m in Flight 3 and 608.67 m in Flight 4. This internal fluctuation in the Mavic sensor had an amplitude of 3.45 m across the flights.

The Phantom system exhibited a similar variation pattern, albeit within a distinct altimetric range. At the same location (X-axis, Position 1), Phantom Flights 1 and 2 recorded mean elevations of 617.20 m and 617.31 m, respectively. However, during Flights 3 and 4, the values decreased to 614.82 m and 614.92 m. When comparing the two platforms, a disparity of approximately 10 m in absolute elevation values was observed; for example, at Position 2 along the X-axis, the Mavic recorded 608.00 m during Flight 1, whereas the Phantom recorded 617.45 m.

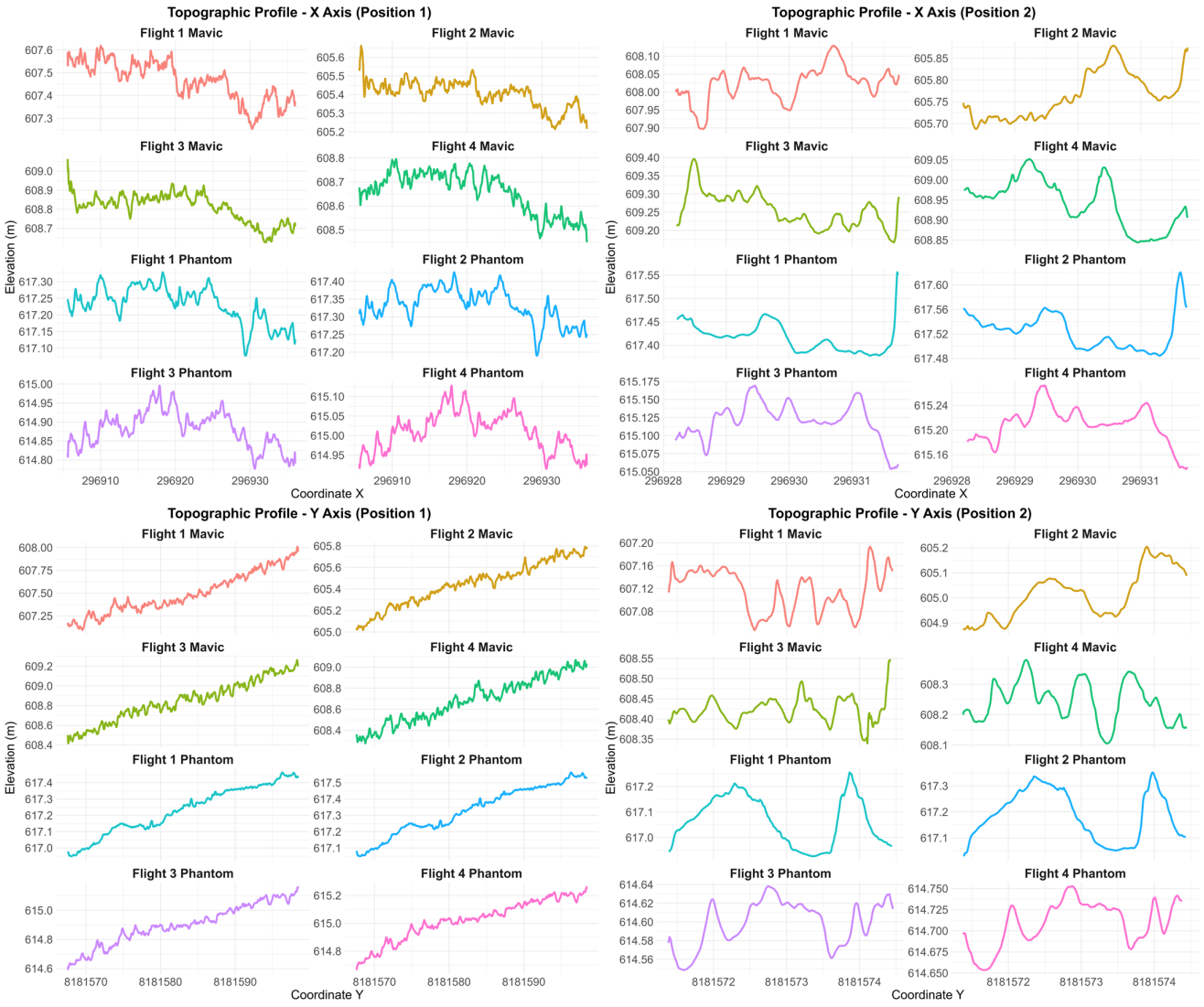

Figure 2. Topographic profiles extracted from DEMs generated by the DJI Mavic 3 Multispectral and the DJI Phantom 4 Multispectral platforms along the X- and Y-axes under pre- and post-harrowing conditions. Although systematic vertical offsets are observed between platforms, similar profile shapes indicate the preservation of terrain morphology and surface microtopography.

Along the Y-axis (Position 1), Mavic Flight 1 started at 607.15 m, confirming the consistency of the observed elevation range. Although differences in absolute elevation values were evident between platforms, the extracted profiles showed similar terrain patterns, including slopes, depressions, and micro-undulations associated with soil preparation. Phantom-derived profiles tended to exhibit smoother surfaces, particularly during pre-harrowing flights, whereas Mavic-derived profiles preserved a greater level of microtopographic detail. Following harrowing, profile shapes became more uniform, and surface continuity improved for both platforms. Furthermore, after mean removal, the relative profiles exhibited strong overlap among flights and platforms, indicating that the evaluated DEMs consistently represented the same terrain morphology. Therefore, the observed differences are primarily associated with systematic vertical offsets (z-shifts) rather than distortions in terrain representation.

3.3. Spatialized Altimetric Mapping

Spatial analysis of the altimetric maps revealed consistent differences in the distribution of relative elevation classes between the models generated by the Mavic and Phantom platforms, in both longitudinal and transversal flights. After normalizing the Digital Elevation Models (DEMs) to the 600 m reference level, the analyses presented the proportional distribution of elevation classes, minimizing interference from absolute differences between platforms.

In longitudinal flights (Figure 3), the models derived from the Mavic platform (Flights 1 and 3) exhibited a predominance of the upper elevation classes (>600.50 m), covering approximately 65% of the total mapped area in both flights. Intermediate classes represented approximately one-third of the surface, whereas the lowest elevations remained restricted to less than 7% of the total area.

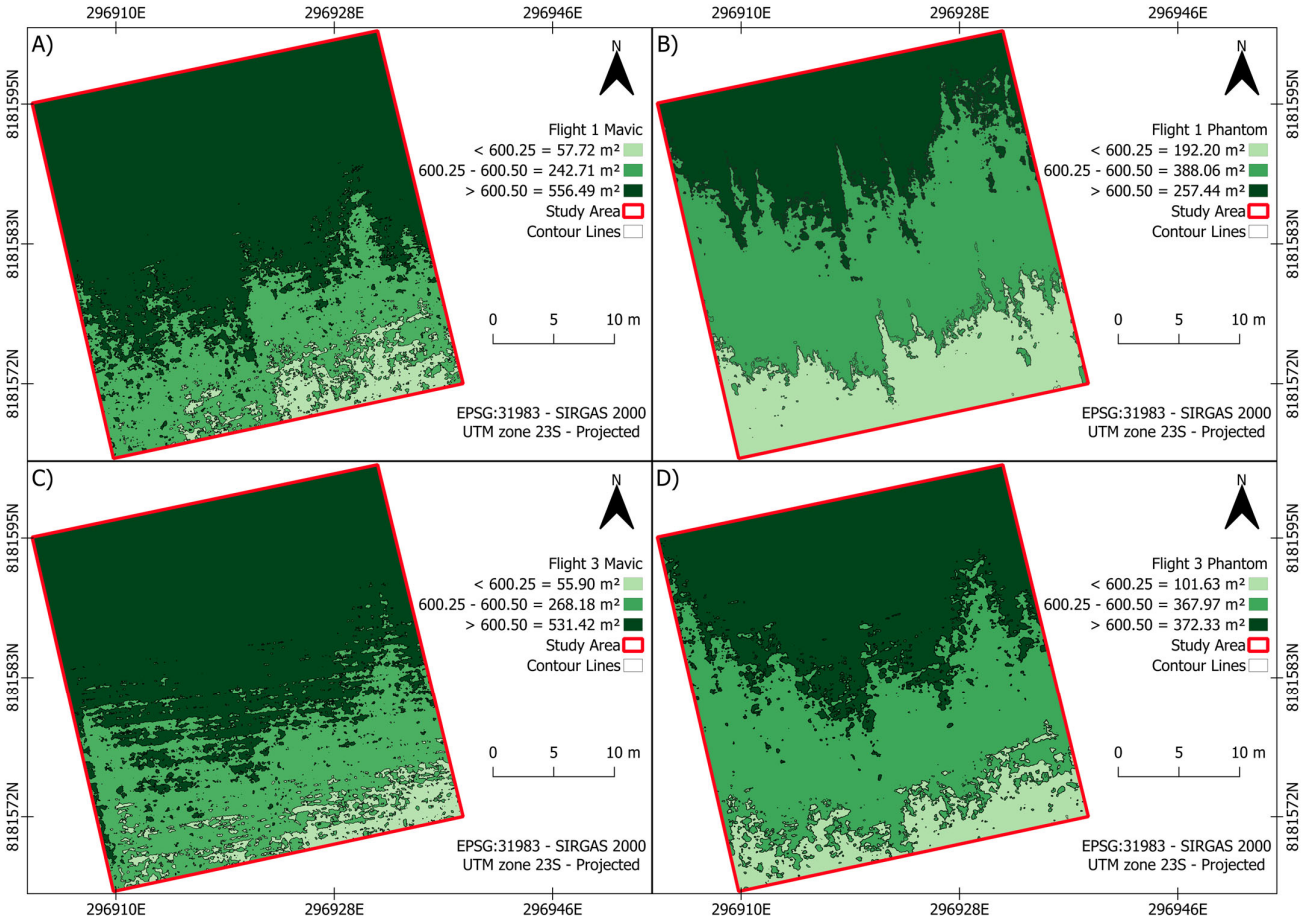

Figure 3. Normalized elevation classes obtained from longitudinal flights using the DJI Mavic 3 Multispectral and the DJI Phantom 4 Multispectral platforms. (**A**) Flight 1 Mavic; (**B**) Flight 1 Phantom; (**C**) Flight 3 Mavic; and (**D**) Flight 3 Phantom. Elevation classes were normalized relative to 600 m.

In contrast, the longitudinal Phantom models exhibited a more balanced distribution among the elevation intervals. In Flight 1 Phantom, approximately half of the area was concentrated in the intermediate class, whereas nearly one-third remained associated with the upper classes. In Flight 3 Phantom, an increase in the proportional participation of the highest relative elevations was observed, approaching the spatial pattern identified in the Mavic models.

In transversal flights (Figure 4), the Mavic models maintained predominance of the upper relative elevation classes. Flight 4 Mavic showed the highest proportion of areas above 600.50 m among all evaluated models, covering approximately 70% of the total surface.

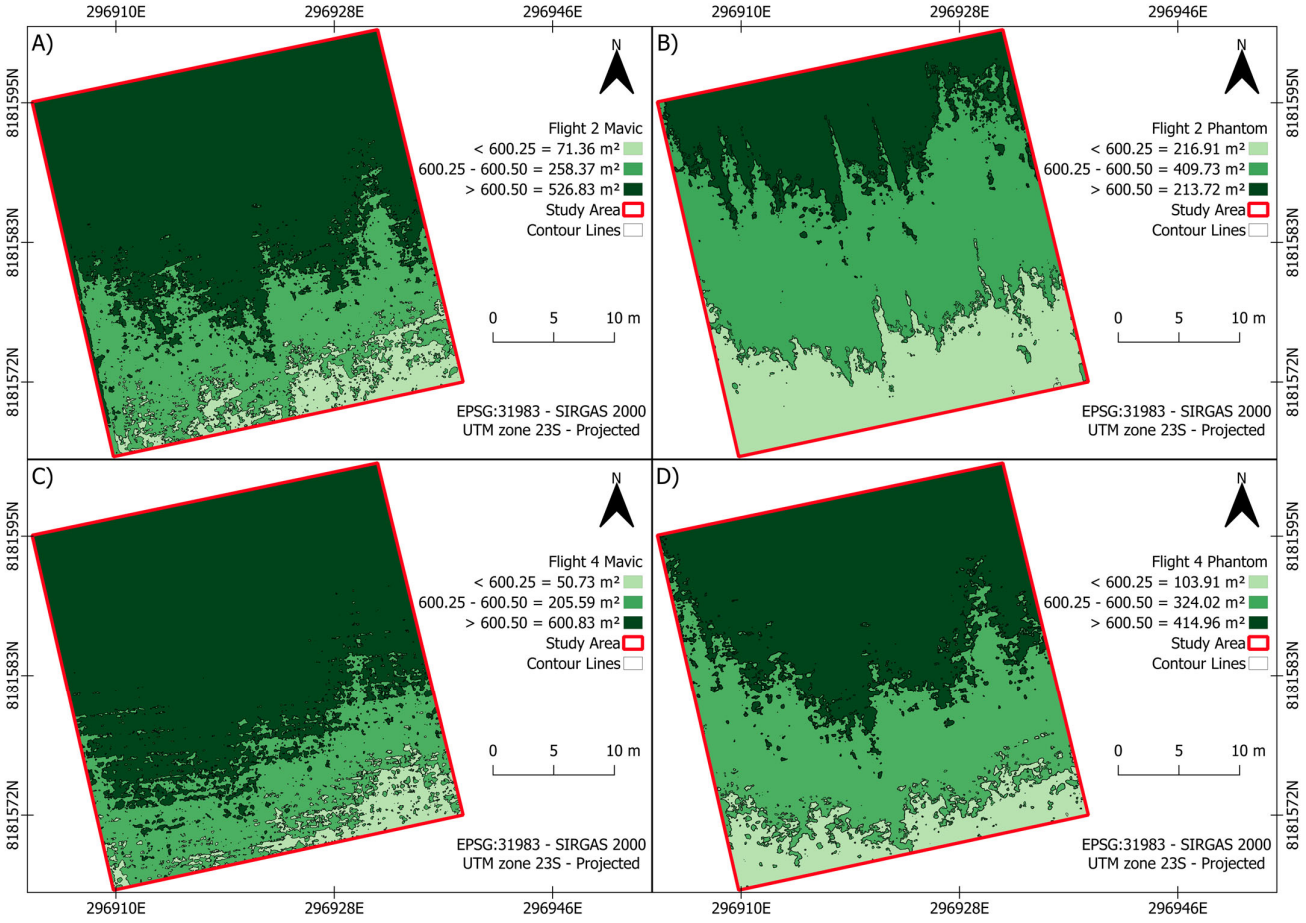

Figure 4. Normalized elevation classes obtained from transversal flights using the DJI Mavic 3 Multispectral and the DJI Phantom 4 Multispectral platforms. (**A**) Flight 2 Mavic; (**B**) Flight 2 Phantom; (**C**) Flight 4 Mavic; and (**D**) Flight 4 Phantom. Elevation classes were normalized relative to 600 m.

The transversal Phantom models exhibited distinct behavior, characterized by a greater balance between intermediate and upper classes. In Flight 2 Phantom, approximately half of the surface remained concentrated within the intermediate range, whereas only about one-quarter of the area was classified within the upper interval. In Flight 4 Phantom, an increase in the proportional participation of the upper classes was observed, accompanied by a relative reduction in intermediate areas. Mavic models showed greater spatial dominance of the upper elevation classes after raster normalization, whereas Phantom models showed a more heterogeneous distribution across the reclassified intervals.

Furthermore, flight direction influenced the spatial distribution of elevation classes. Transversal flights, particularly in the Mavic models, exhibited a greater relative concentration of the upper classes than longitudinal flights. The spatial results corroborate the previously presented statistical analyses, reinforcing that differences between platforms and flight directions directly affect the spatial organization of the Digital Elevation Models.

4. Discussion

4.1. Influence of Platforms and Operational Conditions

The results showed significant differences in elevation values among the Digital Elevation Models generated by the evaluated platforms and flights, with higher mean values in the Phantom models and lower values in the Mavic models. These variations reflect the combined influence of platform characteristics, soil surface conditions, and flight direction on photogrammetric reconstruction and DEM elevation consistency. Similarly, Ref. [27], while evaluating Digital Terrain Models obtained from RPAs in agricultural coffee-growing areas, observed variations among models generated under different acquisition conditions, highlighting differences in elevation values and terrain surface representation.

Within this analytical framework, the observed differences should be interpreted as systematic vertical offsets (z-shifts) rather than actual terrain elevation changes. Although all flights were conducted with RTK operating in fixed mode, the DEMs were generated without ground control points, making the final elevations dependent on onboard GNSS positioning and photogrammetric reconstruction. Differences in sensor characteristics, camera calibration, and image geometry may have contributed to the observed vertical displacement between platforms.

Despite the differences in absolute elevation values, the evaluated models exhibited low internal dispersion and similar surface behavior throughout the experimental area. Furthermore, the topographic profiles demonstrated the preservation of slopes, depressions, and surface micro-undulations, indicating a consistent representation of terrain morphology. The strong overlap observed among normalized profiles further indicates that the differences between platforms were primarily related to vertical offsets rather than changes in terrain shape. Similar results were reported by [28], who, when evaluating Digital Surface Models obtained from RPAs, identified variations among models generated under different acquisition conditions but observed the preservation of the terrain surface's spatial representation. According to the authors, despite the observed differences among the models, the surface relief features remained adequately represented.

Ref. [29], while evaluating surface roughness in agricultural areas using drones, observed that soil surface irregularities could be satisfactorily identified from RPA-acquired imagery, enabling the distinction of spatial patterns related to surface conditions within the area. Furthermore, the authors also observed that more heterogeneous surfaces exhibit greater spatial variability, whereas more homogeneous areas allow improved representation of soil surface patterns.

Ref. [30] found that soil tillage operations directly alter surface roughness, primarily due to clods, furrows, and discontinuities formed by mechanized operations. The authors highlighted that more irregular surfaces exhibit greater surface variability, whereas more uniform areas tend to present more homogeneous behavior in the representation of the soil surface. This behavior is consistent with the present study, where post-harrowing flights showed greater agreement among DEMs and more uniform topographic profiles, suggesting that surface homogenization favored photogrammetric reconstruction.

4.2. Morphological Representation and Preservation of Surface Microtopography

The topographic profiles obtained in this study exhibited high morphological correspondence among the evaluated models, maintaining similar patterns of slopes, depressions, and micro-undulations throughout the experimental area. Even in the presence of the observed elevation differences between platforms, the profiles preserved

the geometric configuration of the represented relief, indicating consistency in the morphological reconstruction of the agricultural surface.

To quantitatively evaluate terrain morphology preservation, Pearson correlation coefficients were calculated between normalized Mavic and Phantom profiles extracted from Position 1 along the Y-axis. Correlation values ranged from 0.84 to 0.96 across the evaluated flights, indicating strong agreement between platforms despite the presence of systematic vertical offsets. These results support the visual interpretation of the profiles and confirm that both RPAs consistently reproduced the same microtopographic patterns. Ref. [31] also demonstrated that RPA-derived models could adequately represent surface terrain morphology, preserving the continuity of topographic features and the geometric coherence of the analyzed area.

The elevation differences observed among the models were mainly associated with absolute elevation values, without significantly altering the morphological behavior of the extracted profiles. The preservation of profile continuity and the correspondence among represented features demonstrate stability in surface reconstruction, indicating that the variations among platforms did not compromise the relative representation of relief throughout the experimental area. Similar findings were reported by [32], who, when comparing RPA-DEM and RPA-DSM models with reference surfaces obtained by ALS, identified elevation differences among the evaluated products while maintaining topographic representation and good spatial correspondence of terrain features among the analyzed models. The results obtained in this study suggest a predominance of systematic vertical displacements (z-shift) between platforms, since the elevation differences occurred mainly in absolute elevation values. In contrast, the relative surface morphology remained preserved throughout the topographic profiles.

Ref. [33] observed that mechanized operations significantly alter agricultural microtopography, forming furrows, ridges, and surface aggregates that modify surface roughness and the spatial organization of the soil surface. The authors further emphasized that these features introduce directional patterns into the disturbed surface, directly influencing the microtopographic variability observed in digital models. Complementarily, Ref. [34] highlighted that RPA-SfM-derived models have a high capability to represent surface irregularities and microtopographic features of agricultural terrain. In this context, the micro-undulations identified across the elevation profiles demonstrate that the generated models could represent local morphological variations associated with mechanized soil preparation, thereby evidencing surface patterns related to furrows, ridges, and aggregates on the disturbed surface.

Ref. [35] demonstrated that digital models derived from photogrammetry adequately preserved surface microtopography and the geometric continuity of agricultural terrain, enabling a consistent representation of morphological features of the soil surface. The high correlation coefficients obtained between normalized profiles reinforce this interpretation, indicating that the observed differences were predominantly related to systematic vertical offsets rather than distortions in terrain morphology. Similar behavior was observed in the profiles obtained in this study, in which surface irregularities and morphological variations remained preserved throughout the extracted topographic sections. These findings suggest that platform-related effects primarily influenced absolute elevation positioning, whereas the photogrammetric reconstruction process remained sufficiently robust to preserve the relative terrain structure and microtopographic patterns across the evaluated DEMs.

4.3. Spatial Organization of Elevation Classes and the Effect of Flight Direction

The normalization of the Digital Elevation Models enabled the identification of distinct spatial behaviors between the models generated by the Mavic and Phantom

platforms, evidencing differences in the organization of elevation classes throughout the experimental area. These spatial differences may be explained by the combined influence of platform characteristics, flight direction, and the interaction between image acquisition geometry and the directional microtopographic patterns created by mechanized soil preparation. Ref. [36] highlighted that analyses derived from high-resolution DEMs enable the interpretation of terrain spatial variability and the identification of patterns associated with surface dynamics.

The observed differences in elevation-class distribution were primarily related to image acquisition geometry rather than changes in terrain morphology. The greater concentration of upper classes in transversal flights may be associated with the orientation of tillage-induced furrows and ridges relative to the flight path, which can influence image matching and surface reconstruction.

Ref. [37], while evaluating agricultural surfaces using RPAs, also observed that areas subjected to mechanized tillage exhibit spatial variations in soil microtopography and surface irregularities. The authors verified that RPA-derived models enable the identification of spatial patterns related to the surface conditions of agricultural terrain, supporting analyses of the spatial organization of disturbed surfaces. The results obtained in the present study are consistent with these findings, indicating that acquisition direction can influence the spatial representation of reconstructed surfaces.

Ref. [38] emphasized that topographic attributes derived from RPA-based Digital Elevation Models, such as elevation, orientation, and spatial variability, contribute to the interpretation of agricultural terrain surface behavior and the spatial distribution of topographic features. Despite differences in class distribution, the overall spatial organization of the terrain was preserved, indicating a consistent surface representation across flight configurations.

The preservation of the spatial continuity of surface features observed in the elevation models demonstrates consistency in the representation of the experimental area surface, enabling the identification of spatial patterns related to microtopography after mechanized preparation. Ref. [39] emphasized that high-resolution elevation models obtained from RPAs allow the representation of terrain surface complexity and the identification of spatial patterns associated with topographic variability within the analyzed area.

Complementarily, Ref. [40] demonstrated that photogrammetric models and DSMs could represent alterations in surface roughness and microtopographic variations, enabling the identification of differences in soil surface conditions. In the context of agricultural mechanization, such information may be used to evaluate the quality of soil preparation operations, since the spatial distribution of surface irregularities directly reflects the effect of implements such as plows and harrows on terrain conformation. Therefore, RPA-derived DEMs represent a valuable tool for monitoring surface roughness and spatial patterns associated with mechanized soil preparation. Taken together, the results demonstrate that platform characteristics, soil surface conditions, and flight direction affect DEM behavior without substantially altering terrain morphology representation.

5. Conclusions

The Digital Elevation Models generated by the DJI Mavic 3 Multispectral and DJI Phantom 4 Multispectral platforms showed significant differences in absolute elevation values, characterized as systematic vertical offsets (z-shifts) rather than actual terrain elevation differences. The DEMs derived from the Phantom platform consistently showed higher values than those from the Mavic platform, indicating systematic vertical displacement between datasets. Despite these discrepancies, all models preserved the

morphological continuity and relative geometry of the agricultural surface, consistently representing microtopographic features associated with mechanized soil preparation. Soil surface conditions and flight direction directly influenced DEM consistency, with post-tillage and longitudinal flights showing greater agreement and more stable altimetric behavior, while transversal flights tended to concentrate higher elevation classes, particularly in the Mavic-derived models.

These results demonstrate that both surface roughness and flight orientation influence the spatial distribution and relative elevation consistency of DEMs. The findings contribute to a better understanding of how platform type, flight direction, and soil surface conditions affect DEM behavior in agricultural environments. However, because no independent ground-reference measurements were available, the results should be interpreted within the scope of comparative DEM evaluation rather than absolute accuracy assessment. Future studies incorporating ground control points, independent elevation references, and additional operational scenarios are required to validate the observed vertical offsets and evaluate the broader applicability of these findings under different agricultural conditions.

Author Contributions: Conceptualization, L.G.M.d.S., L.S.S. and D.S.; methodology, L.G.M.d.S., L.S.S. and D.S.; software, L.G.M.d.S.; validation, L.G.M.d.S., L.S.S., M.D.d.S.L. and D.S.; formal analysis, L.G.M.d.S. and L.S.S.; investigation, L.G.M.d.S., M.D.d.S.L., J.M.d.S. and C.L.d.S.S.; resources, A.P., C.R., D.S. and G.R.; data curation, L.G.M.d.S. and L.S.S.; writing—original draft preparation, L.G.M.d.S.; writing—review and editing, L.S.S., D.S., A.P., C.R. and G.R.; visualization, L.G.M.d.S.; supervision, L.S.S., D.S. and G.R.; project administration, L.S.S. and D.S.; funding acquisition, D.S. and G.R. All authors have read and agreed to the published version of the manuscript.

Funding: This research was funded by FAPEMIG APQ, grant number 00509-24.

Institutional Review Board Statement: Not applicable.

Informed Consent Statement: Not applicable.

Data Availability Statement: The dataset is available upon request from the authors. The data collected by our team for the research can be requested by other researchers for both primary and secondary studies. There are no restrictions on data sharing.

Acknowledgments: The authors gratefully acknowledge the technical support provided by the Institute of Agricultural Sciences (ICA), Federal University of Jequitinhonha and Vale do Mucuri (UFVJM), for granting access to the experimental farm and laboratory facilities, and by the Department of Agriculture Environment Food and Forestry (DAGRI), Biosystem Engineering Division, University of Florence (UniFI). Special thanks to the NEMA research group for their assistance with field data collection and equipment operation. During the preparation of this manuscript, the authors used NotebookLM (Web version powered by Gemini 1.5 Pro, Google, 2025) for the purpose of generating and structuring the graphical abstract. The prompt used was: **"Create a professional graphical abstract for a Q1 scientific paper titled 'Mechanized Ground Roughness Mapping by Remotely Piloted Aircraft'. The layout should follow a 'Problem-Method-Results' flow. Section 1 (Setup): Illustrate two drones (DJI Mavic and Phantom) flying over a tilled field (plowed soil). Section 2 (Method): Flowchart showing RPA Imagery -> SfM Processing -> DEM Generation. Section 3 (Findings): Highlight the 'z-shift' (vertical displacement between drones) while showing that the terrain morphology (curves and furrows) remains the same. Section 4 (Conclusions): Text box stating that longitudinal flights and post-harrowing surfaces yield best results for monitoring tillage quality. Use a palette of agricultural greens, earth tones, and technical blues." The authors have reviewed and edited the output and take full responsibility for the content of this publication.

https://doi.org/10.3390/agriengineering8070256

Conflicts of Interest: The authors declare no conflicts of interest.

References

1. Borah, A.; Sahu, S.; Srivastava, R.P.; Singh, M.; Tyagi, D.B. Exploring the Economic Challenges Threatening Global Agriculture and Food Security. *Ecol. Environ. Conserv.* **2024**, *30*, S193–S199.
2. Pandey, P.C.; Pandey, M. Highlighting the role of agriculture and geospatial technology in food security and sustainable development goals. *Sustain. Dev.* **2023**, *31*, 3175–3195. https://doi.org/10.1002/sd.2600.
3. Taha, M.F.; Mao, H.; Zhang, Z.; Elmasry, G.; Awad, M.A.; Abdalla, A.; Mousa, S.; Elwakeel, A.E.; Elsherbiny, O. Emerging Technologies for Precision Crop Management Towards Agriculture 5.0: A Comprehensive Overview. *Agriculture* **2025**, *15*, 582. https://doi.org/10.3390/agriculture15060582.
4. Vărzaru, A.A. Digital Revolution in Agriculture: Using Predictive Models to Enhance Agricultural Performance Through Digital Technology. *Agriculture* **2025**, *15*, 258. https://doi.org/10.3390/agriculture15030258.
5. Thangamani, R.; Sathya, D.; Kamalam, G.K.; Subramanian, K.M. Farming Beyond Borders: Global Need for Precision Agriculture. In *Internet of Things and Analytics for Agriculture, Volume 4*; Springer: Singapore, 2025; pp. 305–347. https://doi.org/10.1007/978-981-96-7492-3_12.
6. Santana, L.S.; Santos, L.G.M.d.; Silva, J.M.d.; Filho, A.C.M.; Toscano, F.; Silva, E.F.d.F.e.; Jardim, A.M.d.R.F.; Silva, T.G.F.d.; Zanella, M.A. Surface Mapping by RPAs for Ballast Optimization and Slip Reduction in Plowing Operations. *AgriEngineering* **2025**, *7*, 332. https://doi.org/10.3390/agriengineering7100332.
7. Toscano, F.; Fiorentino, C.; Santana, L.S.; Magalhães, R.R.; Albiero, D.; Tomáš, Ř; Klocová, M.; D'Antonio, P. Recent Developments and Future Prospects in the Integration of Machine Learning in Mechanised Systems for Autonomous Spraying: A Brief Review. *AgriEngineering* **2025**, *7*, 142. https://doi.org/10.3390/agriengineering7050142.
8. Fiorentino, C.; D'Antonio, P.; Toscano, F.; Donvito, A.; Modugno, F. New Technique for Monitoring High Nature Value Farmland (HNVF) in Basilicata. *Sustainability* **2023**, *15*, 8377. https://doi.org/10.3390/su15108377.
9. Wu, H.; Li, Y.; Lin, A.; Fan, H.; Fan, K.; Xie, J.; Luo, W. A review of crowdsourced geographic information for land-use and land-cover mapping: Current progress and challenges. *Int. J. Geogr. Inf. Sci.* **2024**, *38*, 2183–2215. https://doi.org/10.1080/13658816.2024.2379468.
10. Selmy, S.A.H.; Kucher, D.E.; Yang, Y.; Jesús García-Navarro, F. Geospatial Data: Acquisition, Applications, and Challenges. In *Exploring Remote Sensing—Methods and Applications*; IntechOpen: London, UK, 2024. https://doi.org/10.5772/intechopen.1006635.
11. Khanal, S.; KC, K.; Fulton, J.P.; Shearer, S.; Ozkan, E. Remote Sensing in Agriculture—Accomplishments, Limitations, and Opportunities. *Remote Sens.* **2020**, *12*, 3783. https://doi.org/10.3390/rs12223783.
12. Dai, W.; Qiu, R.; Wang, B.; Lu, W.; Zheng, G.; Amankwah, S.O.Y.; Wang, G. Enhancing UAV-SfM Photogrammetry for Terrain Modeling from the Perspective of Spatial Structure of Errors. *Remote Sens.* **2023**, *15*, 4305. https://doi.org/10.3390/rs15174305.
13. Jiménez-Jiménez, S.I.; Ojeda-Bustamante, W.; Marcial-Pablo, M.; Enciso, J. Digital Terrain Models Generated with Low-Cost UAV Photogrammetry: Methodology and Accuracy. *ISPRS Int. J. Geo-Inf.* **2021**, *10*, 285. https://doi.org/10.3390/ijgi10050285.
14. Freire-Silva, J.; Miranda Rde, Q.; Candeias, A.L.B. Análise dos Modelos Digitais de Elevação (PE3D, SRTM-30, SRTM-90, ASTER GDEM, TOPODATA, TANDEM-X, ALOS PALSAR e ALOS AW3D30) e a necessidade da produção de dados altimétricos em excelência no Brasil. *Rev. Bras. Geogr. Física* **2022**, *15*, 1543–1555. https://doi.org/10.26848/rbgf.v15.3.p1543-1555.
15. Silva, L.; Conceição, L.A.; Lidon, F.C.; Patanita, M.; D'Antonio, P.; Fiorentino, C. Digitization of Crop Nitrogen Modelling: A Review. *Agronomy* **2023**, *13*, 1964. https://doi.org/10.3390/agronomy13081964.
16. Perna, C.; Pagliai, A.; Sarri, D.; Lisci, R.; Vieri, M. Can a Light Detection and Ranging (LiDAR) and Multispectral Sensor Discriminate Canopy Structure Changes Due to Pruning in Olive Growing? A Field Experimentation. *Sensors* **2024**, *24*, 7894. https://doi.org/10.3390/s24247894.
17. Toscano, F.; Fiorentino, C.; Capece, N.; Erra, U.; Travascia, D.; Scopa, A.; Drosos, M.; D'Antonio, P. Unmanned Aerial Vehicle for Precision Agriculture: A Review. *IEEE Access* **2024**, *12*, 69188–69205. https://doi.org/10.1109/ACCESS.2024.3401018.
18. Bento, N.L.; Ferraz GAe, S.; Santana, L.S.; Faria Rde, O.; Rossi, G.; Bambi, G. Plant Height and Soil Compaction in Coffee Crops Based on LiDAR and RGB Sensors Carried by Remotely Piloted Aircraft. *Remote Sens.* **2025**, *17*, 1445. https://doi.org/10.3390/rs17081445.
19. Deliry, S.I.; Avdan, U. Accuracy of Unmanned Aerial Systems Photogrammetry and Structure from Motion in Surveying and Mapping: A Review. *J. Indian Soc. Remote Sens.* **2021**, *49*, 1997–2017. https://doi.org/10.1007/s12524-021-01366-x.

20. Nakata, Y.; Iwasaki, K.; Shimoda, S.; Torita, H. Understanding microtopography changes in agricultural landscapes through precision assessments of digital surface models by the UAV-RTK-PPK method without ground control points. *Smart Agric. Technol.* **2023**, *5*, 100269. https://doi.org/10.1016/j.atech.2023.100269.
21. Mehmeti, A.; Candido, V.; Canaj, K.; Castronuovo, D.; Perniola, M.; D'Antonio, P.; Cardone, L. Energy, Environmental, and Economic Sustainability of Saffron Cultivation: Insights from the First European (Italian) Case Study. *Sustainability* **2024**, *16*, 1179. https://doi.org/10.3390/su16031179.
22. Ferreira, Z.; Costa, A.C.; Cabral, P. Analysing the spatial context of the altimetric error pattern of a digital elevation model using multiscale geographically weighted regression. *Eur. J. Remote Sens.* **2023**, *56*, 2260092. https://doi.org/10.1080/22797254.2023.2260092.
23. Mohammadi, A.; Karimzadeh, S.; Jalal, S.J.; Kamran, K.V.; Shahabi, H.; Homayouni, S.; Al-Ansari, N. A Multi-Sensor Comparative Analysis on the Suitability of Generated DEM from Sentinel-1 SAR Interferometry Using Statistical and Hydrological Models. *Sensors* **2020**, *20*, 7214. https://doi.org/10.3390/s20247214.
24. Santos Santana, L.; Araújo e Silva Ferraz, G.; Airane dos Santos, S.; Ellen Lima Dias, J. Precision coffee growing: A review. *Coffee Sci.* **2022**, *17*, e172007. https://doi.org/10.25186/.v17i.2007.
25. Bento, N.L.; Silva Ferraz, G.A.e.; Santana, L.S.; de Oliveira Faria, R.; da Silva Amorim, J.; de Lourdes Oliveira e Silva, M.; Silva, M.M.A.; Alonso, D.J.C. Soil compaction mapping by plant height and spectral responses of coffee in multispectral images obtained by remotely piloted aircraft system. *Precis. Agric.* **2024**, *25*, 729–750. https://doi.org/10.1007/s11119-023-10090-0.
26. Santana, L.S.; Ferraz, G.A.e.S.; Cunha, J.P.B.; Santana, M.S.; Faria, R.d.O.; Marin, D.B.; Rossi, G.; Conti, L.; Vieri, M.; Sarri, D. Monitoring Errors of Semi-Mechanized Coffee Planting by Remotely Piloted Aircraft. *Agronomy* **2021**, *11*, 1224. https://doi.org/10.3390/agronomy11061224.
27. Santana, L.S.; Ferraz, G.A.e.S.; Marin, D.B.; Faria, R.d.O.; Santana, M.S.; Rossi, G.; Palchetti, E. Digital Terrain Modelling by Remotely Piloted Aircraft: Optimization and Geometric Uncertainties in Precision Coffee Growing Projects. *Remote Sens.* **2022**, *14*, 911. https://doi.org/10.3390/rs14040911.
28. Czapiewski, S. Assessment of the Applicability of UAV for the Creation of Digital Surface Model of a Small Peatland. *Front. Earth Sci.* **2022**, *10*, 834923. https://doi.org/10.3389/feart.2022.834923.
29. Hieu Luu, T.; Thanh Tam, N.; Nguyen Ky Phuc, P.; Cuong Nguyen, H.; van Le, L.; Hieu Ngo, Q. Evaluation of land roughness and weather effects on paddy field using cameras mounted on drone: A comprehensive analysis from early to mid-growth stages. *J. King Saud Univ. Comput. Inf. Sci.* **2023**, *35*, 101853. https://doi.org/10.1016/j.jksuci.2023.101853.
30. Azizi, A.; Abbaspour-Gilandeh, Y.; Mesri-Gundoshmian, T.; Farooque, A.A.; Afzaal, H. Estimation of Soil Surface Roughness Using Stereo Vision Approach. *Sensors* **2021**, *21*, 4386. https://doi.org/10.3390/s21134386.
31. Park, K.; Shibuo, Y.; Katayama, J.; Baba, S.; Furumai, H. Applicability of High-Resolution Geospatial Data Obtained by UAV Photogrammetry to Develop Drainage System Models for Pluvial Flood Analysis. *J. Disaster Res.* **2021**, *16*, 371–380. https://doi.org/10.20965/jdr.2021.p0371.
32. Szypuła, B. Accuracy of UAV-based DEMs without ground control points. *GeoInformatica* **2024**, *28*, 1–28. https://doi.org/10.1007/s10707-023-00498-1.
33. Liu, L.; Bi, Q.; Zhang, Q.; Tang, J.; Bi, D.; Chen, L. Evaluation Method of Soil Surface Roughness after Ditching Operation Based on Wavelet Transform. *Actuators* **2022**, *11*, 87. https://doi.org/10.3390/act11030087.
34. Straffelini, E.; Cucchiaro, S.; Tarolli, P. Mapping potential surface ponding in agriculture using UAV-SfM. *Earth Surf. Processes Landf.* **2021**, *46*, 1926–1940. https://doi.org/10.1002/esp.5135.
35. Gilliot, J.M.; Vaudour, E.; Michelin, J. Soil surface roughness measurement: A new fully automatic photogrammetric approach applied to agricultural bare fields. *Comput. Electron. Agric.* **2017**, *134*, 63–78. https://doi.org/10.1016/j.compag.2017.01.010.
36. Xiong, L.; Li, S.; Tang, G.; Strobl, J. Geomorphometry and terrain analysis: Data, methods, platforms and applications. *Earth-Sci. Rev.* **2022**, *233*, 104191. https://doi.org/10.1016/j.earscirev.2022.104191.
37. Nakata, Y.; Hayamizu, M.; Ishiyama, N. Spatiotemporal Monitoring of Large Woody Debris Mobility and Distribution Using Unmanned Aerial Vehicles Along the Oshirarika River, Northern Japan. *Drones* **2025**, *9*, 655. https://doi.org/10.3390/drones9090655.
38. Bannari, A.; Selouani, A.; El-Basri, M.; Rhinane, H.; El-Harti, A.; El-Ghmari, A. Multi-Scale Analysis of DEMs Derived from Unmanned Aerial Vehicle (UAV) in Precision Agriculture Context. In Proceedings of the 2021 IEEE International Geoscience and Remote Sensing Symposium IGARSS, Brussels, Belgium, 11–16 July 2021; pp. 8285–8288. https://doi.org/10.1109/IGARSS47720.2021.9554020.

39. Grube, G.; Talbot, B.; Grigolato, S. Automated terrain roughness assessment using remotely sensed data. *Int. J. For. Eng.* **2025**, *36*, 299–314. https://doi.org/10.1080/14942119.2025.2480009.
40. Herodowicz-Mleczak, K.; Piekarczyk, J.; Ratajkiewicz, H.; Nowosad, J.; Śledź, S.; Kaźmierowski, C.; Królewicz, S.; Kierzek, R. Estimation of Soil Surface Roughness Parameters Under Simulated Rainfall Using Spectral Reflectance in Optical Domain. *Earth Space Sci.* **2023**, *10*, e2022EA002642. https://doi.org/10.1029/2022EA002642.